Electronic Supplementary Material (ESI) for Inorganic Chemistry Frontiers.

Supplementary Information

Controllable phase transition dependent photoi nduced charge separation in $CuFe_2O_4$ for phot ocatalytic hydrogen evolution

Dongfen Hou, ‡ Jingqi Tian, ‡ Jingying Wei, Dailing Jia, Ke Ma, Huaiguo Xue and Tengfei Jiang*

School of Chemistry and Chemical Engineering, and Institute for Innovative

Materials and Energy, Yangzhou University, 180 Si-Wang-Ting Road, Yangzhou

225002, P. R. China;

*Corresponding Author

Email: jiangtengfei@yzu.edu.cn

Materials

All the chemicals used in this study were of analytical grade and used without further purification. Iron(III) nitrate nonahydrate ($FeNO_3 \cdot 9H_2O$), Copper(II) Nitrate Trihydrate($CuNO_3 \cdot 3H_2O$), Citric acid($C_6H_8O_7$), Urea(CH_4NO_2)were purchased from Sigma-Aldrich Pte. Ltd. (Singapore). The water used throughout all experiments was purified using a Millipore system.

Structural characterisation and performance testing

Scanning electron microscopy (SEM) and X-ray spectroscopy (EDS): The micro-surface morphology of $CuFe_2O_4$ was observed by field emission scanning electron microscopy (FESEM) using an accelerating voltage of 5 kV.

Scanning Electron Microscopy (SEM) and X-ray Spectroscopy (EDS): The micro-surface morphology of $CuFe_2O_4$ was observed by SEM using an accelerating voltage of 5 kV. The energy spectra of the material were scanned using a voltage of 20 kV.

X-ray diffraction (XRD): X-ray diffraction was used to characterise the crystal structure of the powders with diffraction angles (2□) ranging from 10° to 80° at a scanning rate of 2°-min-1. UV-vis-NIR: The absorbance of the material was scanned by UV-vis-NIR spectrometry at wavelengths of 200-2000 nm. X-ray photoelectron spectroscopy (XPS): The chemical composition and state of the material surface were tested by X-ray photoelectron spectroscopy. The sample powder (20 mg) was pressed and cut to a size of about 5 × 5 mm and adhered to a sample tray with double-sided adhesive, and a neutralisation gun was used to eliminate uneven charging and poor conductivity by using a monochromated Al K-α target (1486.6 eV), and the tests were carried out within the full-energy and narrow-energy spectra of 150 eV and 30 eV, with step sizes of 1 eV and 0.05 eV, respectively, and the results were obtained by C 1s spectroscopy. The results were corrected by the 284.8 eV peak of the C 1s spectrum.

Photoelectrochemical tests: the photoelectrochemical responses of these photocatalysts were recorded on an Autolab electrochemical workstation using a 500 W xenon lamp with a light intensity of 100 mW/cm^2. working electrodes were fabricated using the drop-coating method. The photocatalyst sample (8 mg) was added to ethylene glycol methyl ether (3 mL) and sonicated for 30 min. The sample suspension was then drop-coated onto a fluorine-doped tin oxide (FTO, 1 × 3 cm^2) substrate and heated at 90 °C until the solution evaporated to form a film. Then the film was burned in a tube furnace at 200 ℃ for 30 min under nitrogen atmosphere with a heating rate of 3 ℃/min. The photoelectrochemical properties were tested in 0.5 mo/L Na_2SO_4 electrolyte with a platinum wire and saturated Ag/AgCl as counter electrode and reference electrode, respectively.

The intensity of steady-state photoluminescence (PL) spectra was used to qualitatively monitor the separation or complexation efficiency of the photocatalysts, and surface

photovoltaic spectroscopy (SPV) provides information on the variation of surface photovoltaics with respect to the energy of the incident photons.The surface photovoltaic spectroscopy test system was implemented based on a lock-in amplifier, which consisted of a 500 W xenon lamp source (CHF-XM500, Beijing Trusttech Co. Ltd.), a monochromator (SBP500, Zolix), a lock-in amplifier (SR830, Stanford Research Systems, Inc.), a modulation fan (SR540, Stanford Research Systems, Inc.), and a sample cell. The monochromator was modulated at 23 Hz, and its intensity depended on the intensity energy distribution of the xenon lamp source used. The monochromator and lock-in amplifier were controlled by a computer, and the input impedance of the lock-in amplifier was 10 M□. The surface photovoltaic spectrum is swept from long to short waves during scanning, and a UV cut-off filter (□ > 420 nm) is used to remove the octave light generated by the grating monochromator when the wavelength of the monochromatic light is greater than 600 nm. The entire test system was calibrated with a silicon detector (DSI200, Zolix) to eliminate phase differences caused by the non-photovoltaic response, so that the measured phase values truly reflect the kinetic characteristics of the photovoltaic signal.

Photocatalytic reaction: 10 mg of photocatalyst (without co-catalyst) was dispersed in 9 mL of aqueous solution, 1 mL of methanol was used as a sacrificial agent, and nitrogen was used to replace the gas for 5 min. The suspension was continuously stirred for 4 h during the photocatalytic reaction, and the bottom was irradiated by a 500 W xenon lamp, and detected by a gas chromatograph (GC-2014, Shimadzu, with nitrogen as the carrier gas) using a thermal conductivity detector (TCD). Hydrogen generation.

Catalysts deposition was conducted as follow: H_2PtCl_6 (1 wt% based on Pt atoms) was was add into the solution, after irradiated with light for 1 h to ensure Pt was in-situ deposited on the surface of $CuFe_2O_4$ and subsequently washing and drying of the catalyst.The dried catalyst is put into the system of photocatalytic hydrogen production.

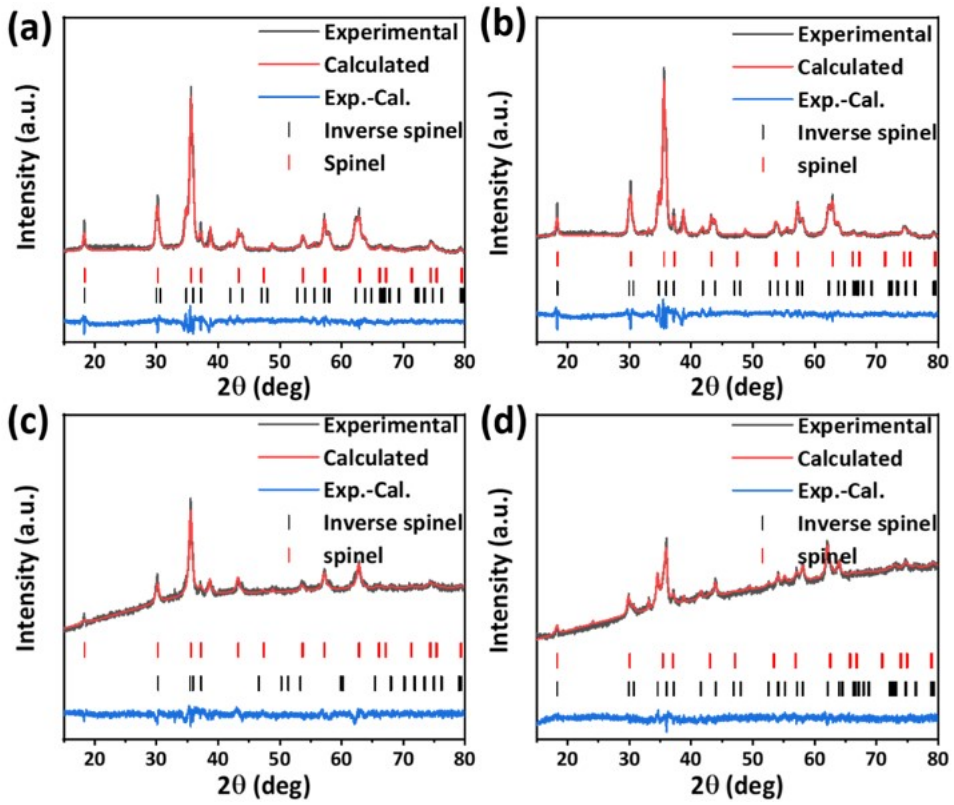

Fig S1.(a) XRD Rietveld analysis of CFO-400;(b) XRD Rietveld analysis of CFO-425; (c) XRD Rietveld analysis of CFO-450; (d) XRD Rietveld analysis of CFO-550.

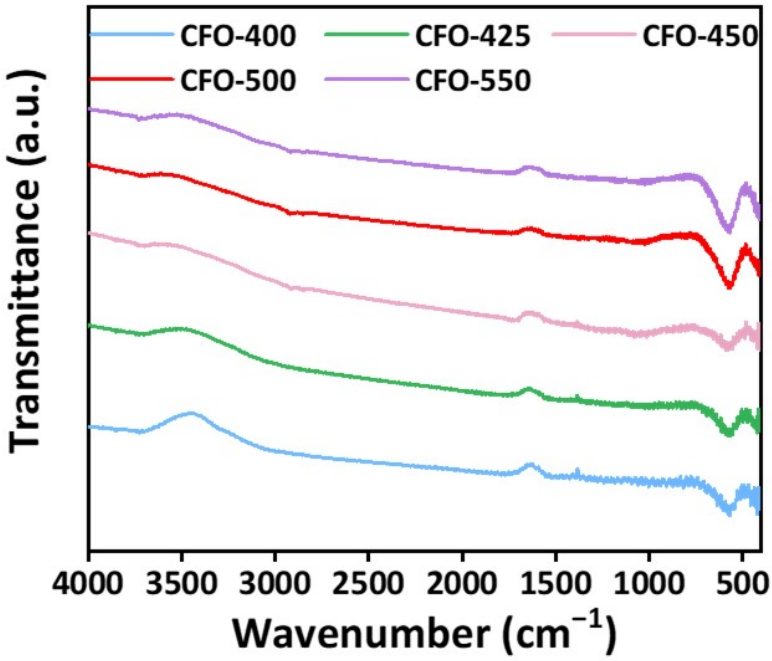

Fig S2. FTIR spectra of CFO-400.CFO-425;CFO-450;CFO-500;CFO-550.

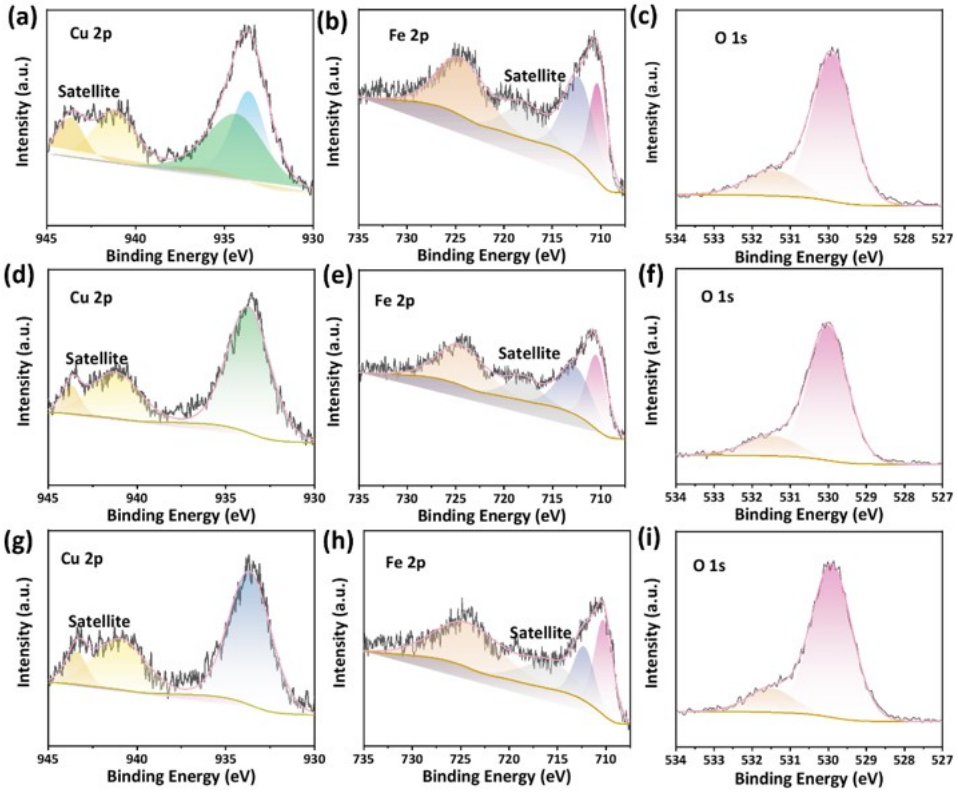

Fig S3.(a) Cu 2p spectrum of CFO-425; (b) Fe 2p spectrum of CFO-425;(c) O 1s spectrum of CFO-425; (d) Cu 2p spectrum of CFO-450; (e) Fe 2p spectrum of CFO-450;(f) O 1s spectrum of CFO-450; (g) Cu 2p spectrum of CFO-550; (h) Fe 2p spectrum of CFO-550;(i) O 1s spectrum of CFO-550.

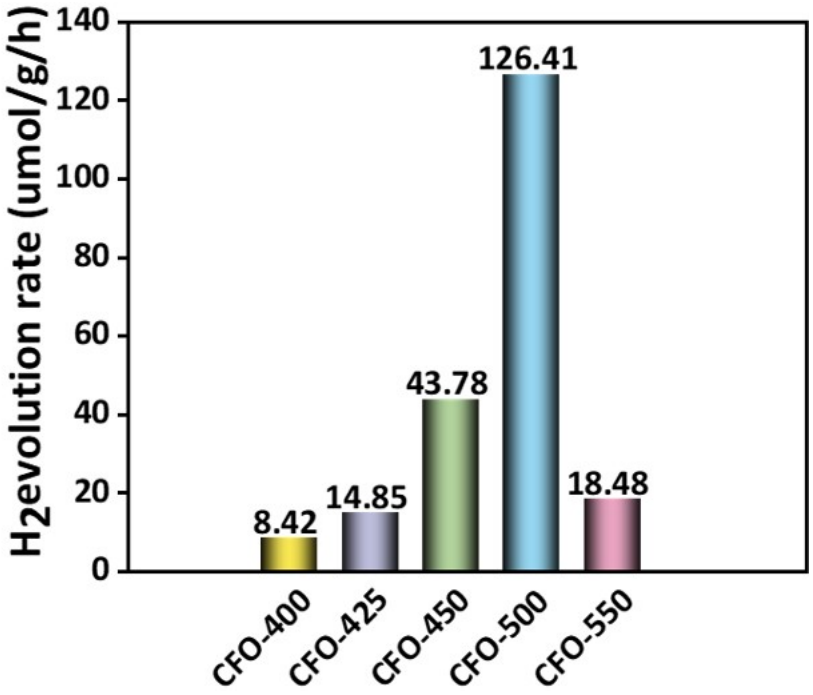

Fig S4. Comparison of catalytic activity of gases produced by different samples.

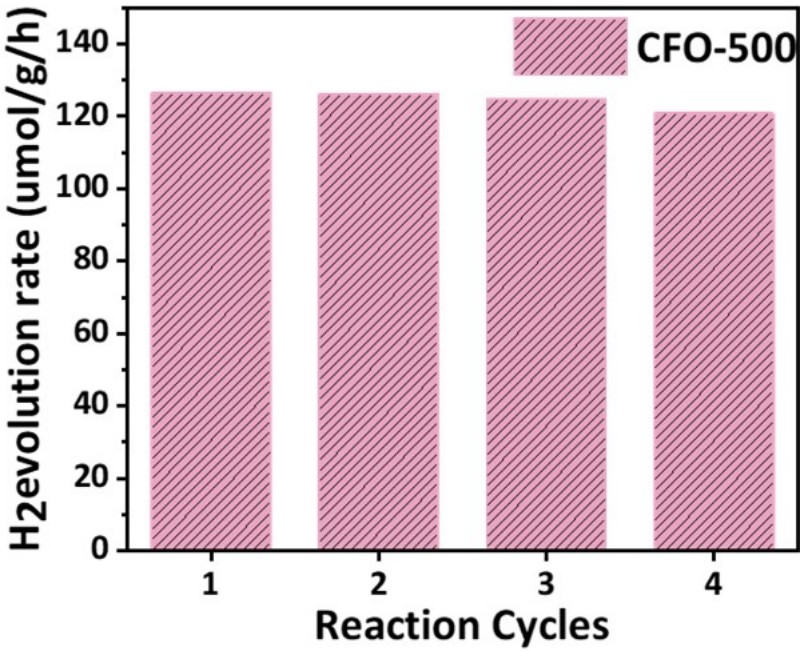

Fig S5. Four consecutive stability tests for hydrogen production from CFO-500 under illumination.

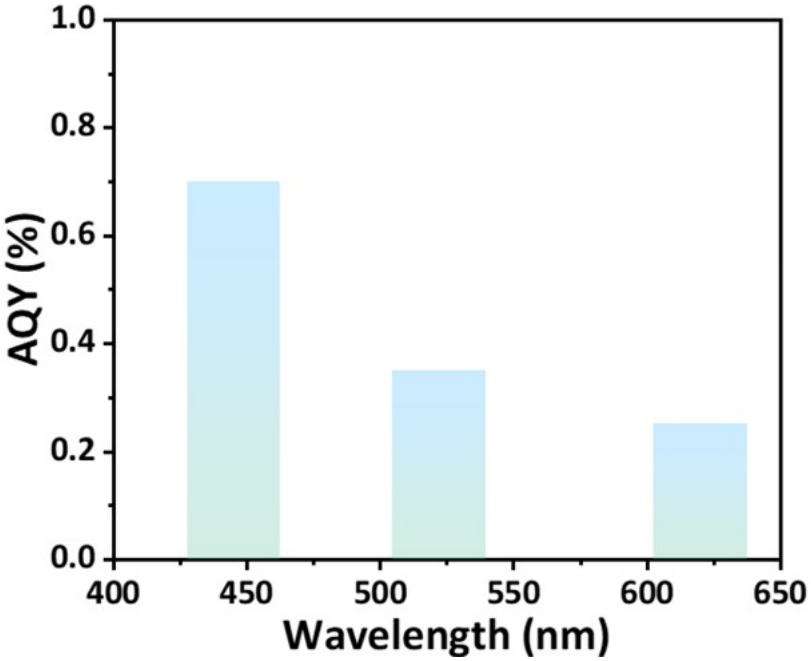

Fig S6. Apparent quantum yield (AQY) of CFO-500.

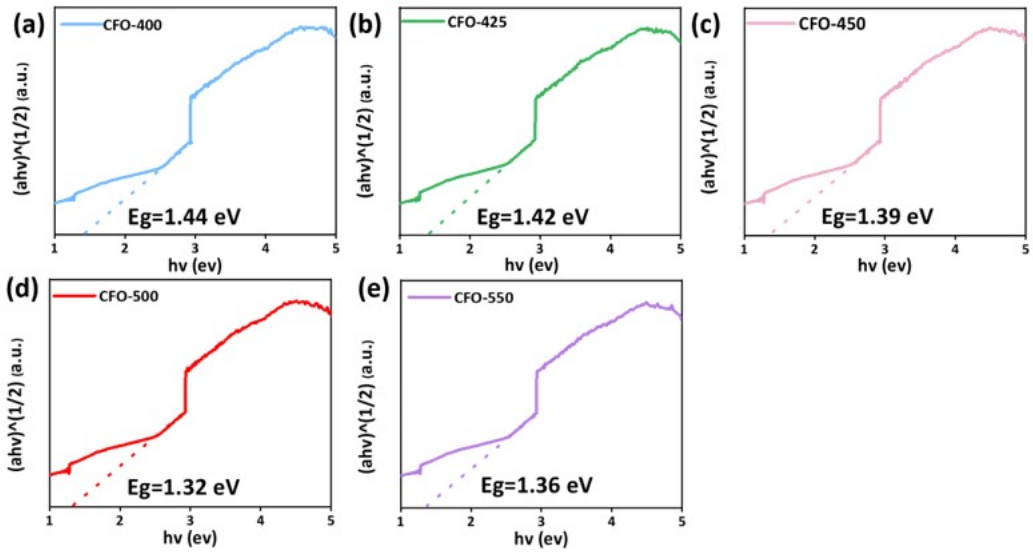

Fig S7. Tauc diagrams for CFO-400, CFO-425, CFO-450, CFO-500, CFO-550, CFO-400.

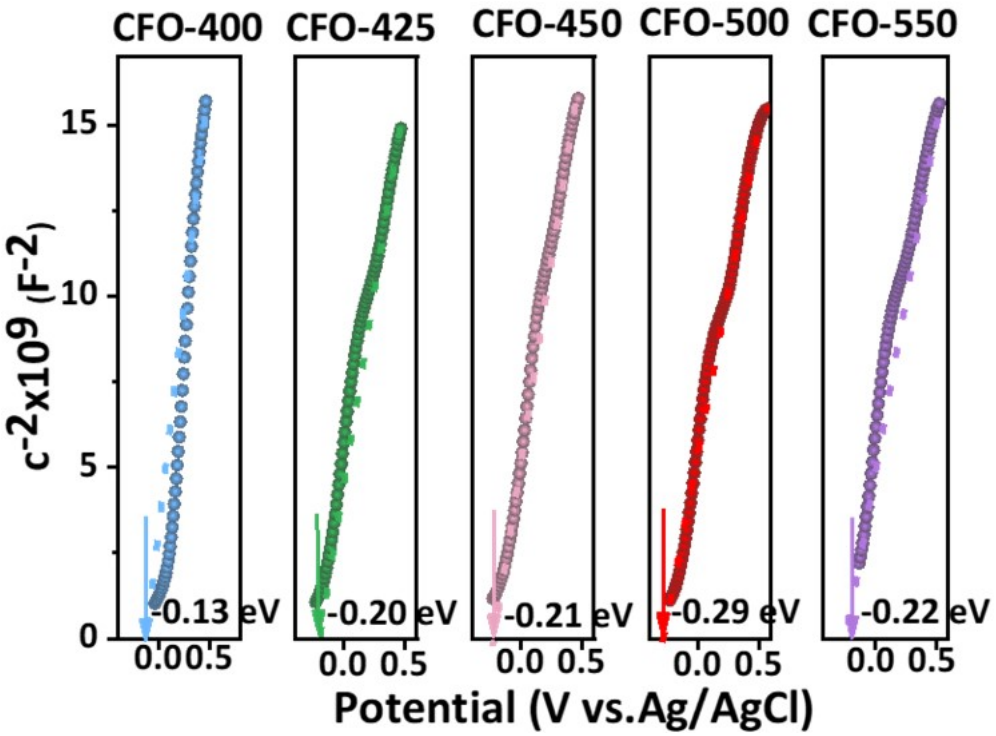

Fig S8. Mott-Schottky plots of CFO-400, CFO-425, CFO-450, CFO-500, CFO-550.

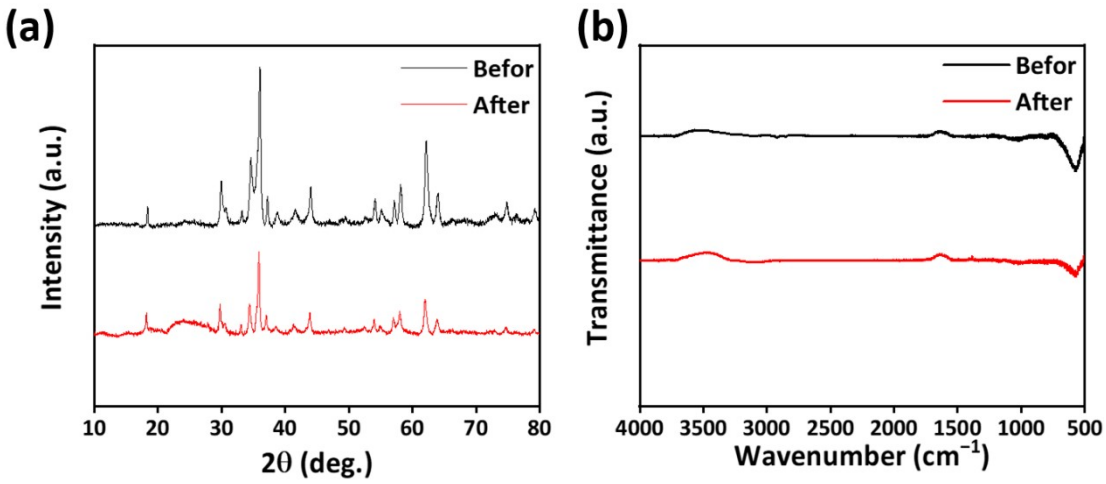

Fig S9. XRD pattern, FT-IR spectra of CFO-500 before and after photocatalytic hydrogen evolution.

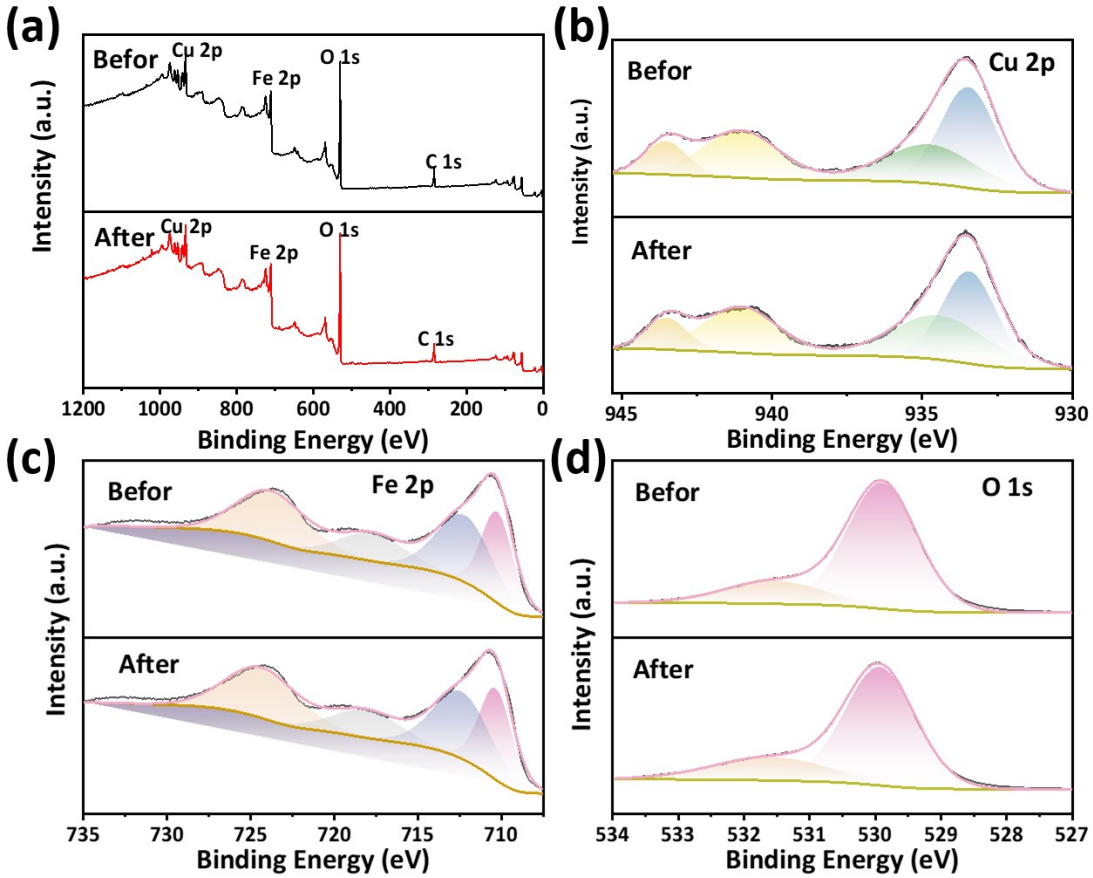

Fig S10. XPS spectra of CFO-500 before and after photocatalytic hydrogen evolution.

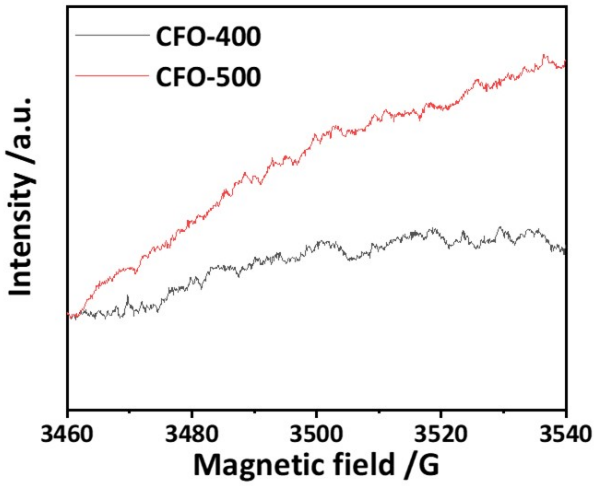

Fig S11.EPR spectra of CFO-400 and CFO-500.

Table S1 Refined structural parameters of CFO.

T(K)	atom	site	x	y	z
400	Cu	8d	0.00000	0.00000	0.50000
	Fe1	8d	0.00000	0.00000	0.50000
	Fe2	4a	0.00000	0.75000	0.12500
	O	16h	0.00000	0.01168	0.24819
Space group: I41/amd ,Rexp = 1.89%, Rwp =4.55%.					
T(K)	atom	site	x	y	z
400	Cu	16d	0.62500	0.62500	0.62500
	Fe1	16d	0.62500	0.62500	0.62500
	Fe2	8a	0.00000	0.00000	0.00000
	O	32e	0.37731	0.37731	0.37731
Space group: Fd-3m,Rexp = 1.89%, Rwp =4.55%.					
T(K)	atom	site	x	y	z
425	Cu	8d	0.00000	0.00000	0.50000
	Fe1	8d	0.00000	0.00000	0.50000
	Fe2	4a	0.00000	0.75000	0.12500
	O	16h	0.00000	0.00984	0.25192
Space group: I41/amd ,Rexp = 1.88%, Rwp =4.80%.					
T(K)	atom	site	x	y	z
425	Cu	16d	0.62500	0.62500	0.62500
	Fe1	16d	0.62500	0.62500	0.62500
	Fe2	8a	0.00000	0.00000	0.00000
	O	32e	0.37644	0.37644	0.37644
Space group: Fd-3m,Rexp = 1.88%, Rwp =4.80%.					
T(K)	atom	site	x	y	z
450	Cu	8d	0.00000	0.00000	0.50000
	Fe1	8d	0.00000	0.00000	0.50000
	Fe2	4a	0.00000	0.75000	0.12500
	O	16h	0.00000	0.12772	0.0344
Space group: I41/amd ,Rexp = 1.88%, Rwp =4.33%.					
T(K)	atom	site	x	y	z

450	Cu	16d	0.62500	0.62500	0.62500
	Fe1	16d	0.62500	0.62500	0.62500
	Fe2	8a	0.00000	0.00000	0.00000
	O	32e	0.36773	0.36773	0.36773
Space group: Fd-3m,Rexp = 1.88%, Rwp =4.33%.					
T(K)	atom	site	x	y	z
500	Cu	8d	0.00000	0.00000	0.50000
	Fe1	8d	0.00000	0.00000	0.50000
	Fe2	4a	0.00000	0.75000	0.12500
	O	16h	0.00000	0.01536	0.25839
Space group: I41/amd ,Rexp = 1.92%, Rwp =4.95%.					
T(K)	atom	site	x	y	z
500	Cu	16d	0.62500	0.62500	0.62500
	Fe1	16d	0.62500	0.62500	0.62500
	Fe2	8a	0.00000	0.00000	0.00000
	O	32e	0.35440	0.35440	0.35440
Space group: Fd-3m,Rexp = 1.92%, Rwp =4.95%.					
T(K)	atom	site	x	y	z
550	Cu	8d	0.00000	0.00000	0.50000
	Fe1	8d	0.00000	0.00000	0.50000
	Fe2	4a	0.00000	0.75000	0.12500
	O	16h	0.00000	0.01003	0.24964
Space group: I41/amd ,Rexp = 1.25%, Rwp =4.69%.					
T(K)	atom	site	x	y	z
550	Cu	16d	0.62500	0.62500	0.62500
	Fe1	16d	0.62500	0.62500	0.62500
	Fe2	8a	0.00000	0.00000	0.00000
	O	32e	0.36666	0.36666	0.36666
Space group: Fd-3m,Rexp = 1.25%, Rwp =4.69%.					

Table S2 Lattice and defective oxygen content of CFO obtained by XPS spectral fitting of Ols.

Sample	Lattice O(%)	Defect(%)
CFO-400	73.74	26.76
CFO-425	76.73	23.27
CFO-450	76.50	23.50
CFO-500	62.77	37.23
CFO-550	82.99	17.01

Table S3 Fitting results of Nyquist plots for samples.

Sample	R_s (Ω)	R_{ct} (Ω)	Q(F)	n	C(F)
CFO-400	34.38	2134900	4.956×10^{-7}	0.94155	4.9734×10^{-7}
CFO-425	18.31	879600	1.6624×10^{-6}	0.89624	1.6800×10^{-6}
CFO-450	22.87	143520	2.9061×10^{-6}	0.84741	2.4827×10^{-6}
CFO-500	40.86	132410	1.157×10^{-5}	0.83907	1.2556×10^{-5}
CFO-550	31.15	193620	9.7414×10^{-6}	0.90063	1.0448×10^{-5}

Table S4 Comparison of band gap, conduction band and valence band of the samples.

Sample	E_g	E_{CB}(vs.NHE)	E_{vB}(vs.NHE)
CFO-400	1.44 eV	0.09 V	1.53 V
CFO-425	1.42 eV	0.02 V	1.44 V
CFO-450	1.39 eV	0.01 V	1.40 V
CFO-500	1.32 eV	-0.07V	1.25 V
CFO-550	1.36 eV	0 V	1.36 V

Table S5 Comparison of photocatalytic HER performance over various photocatalysts and reaction conditions reported in reference.

Catalysis	sacrificial agent	light source	Activity Rate/ μmol g^{-1} h^{-1}	Ref.
$ZnFe_2O_4$	methanol	300 W xenon lamp	9.61 μmol g^{-1}	[1]
TiO_2@$ZnFe_2O_4$	methanol	300 W xenon lamp	194.61 μmol g^{-1}	[1]
$NiFe_2O_4$	methanol	250 W mercury vapor lamp	317 μmol g^{-1}	[2]
$CuFe_2O_4$	0.25 M Na_2SO_3 – 0.35 Na_2S	300 W xenon lamp	336μmol $g^{-1}h^{-1}$	[3]
$NiFe_2O_4$	0.25 M Na_2SO_3 – 0.35 Na_2S	300 W xenon lamp	234 μmol g^{-1} h^{-1}	[3]
WO_3@ $NiFe_2O_4$	-	500 W xenon lamp	288μmol g^{-1} h^{-1}	[4]
$CoFe_2O_4$	TEOA（10vol %）	5W LED	2.27μmol h^{-1}	[5]
$CoFe_2O_4$ /$NiMoO_4$	TEOA（10vol %）	5W LED	16.84μmol h^{-1}	[5]
TiO_2/$FePS_3$	ethanol	350 W xenon lamp	99.5μmol g^{-1} h^{-1}	[6]
TiN/N-TiO_2	AA	300 W xenon lamp	703μmol h^{-1}	[7]
Pt-VO-TiO_2	TEOA	300 W xenon lamp	64.5 mmol g^{-1} h^{-1}	[8]
CeCo1:2/P	TEOA	5W LED	486.99μmol	[9]
Ru/g-C_3N_4−x	-	Xe lamp irradiation (200 mW·cm^{-2})	6.42mmol g^{-1} h^{-1}	[12]
$ZnIn_2S_4$/Mo_2TiC_2	TEOA	300 W xenon lamp	3.12 mmol g^{-1} h^{-1}	[13]
$ZnIn_2S_4$/TiO_{2-x}	methanol	300 W xenon lamp	581.1μmol g^{-1} h^{-1}	[14]
Cu_2WS_4/$NiTiO_3$	0.35 mol/L Na_2S and 0.35 mol/L Na_2SO_3	300 W xenon lamp	810 μmol g^{-1} h^{-1}	[15]
CdS/np-rGO	0.35 mol/LNa_2S and Na_2SO_3	300 W xenon lamp	2171.23μmol g^{-1} h^{-1}	[16]
$CuFe_2O_4$	methanol	300 W xenon lamp	126.41μmol g^{-1} h^{-1}	This work

Table S6 photocatalytic H_2 evolution rates of CFO-500 and CFO-500/Pt.

Samples	H_2 evolution rates ($\mu molg^{-1}h^{-1}$)
CFO-500	126.41
CFO-500/Pt	286.20

Calculation

The measurement of apparent quantum efficiency The apparent quantum efficiency (AQE) was also tested under the similar photocatalytic reaction conditions except that the light source was equipped with different band-pass filters for different wavelengths. The amount of the CFO-500. sample was 10 mg. The respective AQE was figured out by the following formula: amount of reacted electrons

$$\mathrm{AQE} = \frac{2\ number\ of\ hydrogenmolecules}{number\ of\ incident\ photons} \times 100\%$$

$$= \frac{1.2 \times 10^8 \times v \times K}{1 \times A \times \lambda} \times 100\%$$

Where H_2Ns, E, and hν represent hydrogen evolution amount, Avogadro constant, light energy in the testing time and irradiation area, and photon energy, respectively.
The equivalent capacitance of the CPE element in R||C is: C=(R × Q)1/n /R

DFT Calculation.

The electronic structure of the system was investigated based on the DFT approach with the CASTEP program. Structure was optimized at the generalized gradient approximation (GGA) level with the Perdew−Burke−Ernzerhof (PBE) exchange−correlation functional and ultrasoft pseudopotentials. To obtain the density of states (DOS) of$CuFe_2O_4$, For geometry optimization, ultrasoft pseudopotentials were used with a kinetic energy cutoff of 351 eV and a G-centered 2× 2 × 1 k-point mesh for sampling the Brillouin zone. During optimization, the lattice parameters were fixed and only the atoms were allowed to relax. The vacuum layer of the models is set at 15 Å to minimize the interaction between the periodicImages.
The d-band centers (εd) were calculated using the following formula:

$$\frac{\int ED_d(E)dE}{\int D_d(E)dE}$$

where D_d(E) represents the density of states (DOS) for the d-orbital .The integration ranges for all calculations were set from 0 eV to 5 eV. we calculated the d-band center of the Fe3d metal atoms and the Cu3d metal atoms.

Reference

1 D. Zeng, J. Wang, Y. Xie, Y. Ling, J. Zhao, H. Ye and T. Chen, TiO_2@$ZnFe_2O_4$ heterojunctions for effecicent photocatalytic degradation of persistent pollutants and hydrogen evolution, *Materials Chemistry and Physics*, 2022, **277**, 125462.

2 J. L. Domínguez-Arvizu, J. A. Jiménez-Miramontes, J. M. Salinas-Gutiérrez, M. J. Meléndez-Zaragoza, A. López-Ortiz and V. Collins-Martínez, Optical properties determination of $NiFe_2O_4$ nanoparticles and their photocatalytic evaluation towards hydrogen production, *International Journal of Hydrogen Energy*, 2017, **42**, 30242–30248.

3 A. Soto-Arreola, A. M. Huerta-Flores, J. M. Mora-Hernández and L. M. Torres-Martínez, Comparative study of the photocatalytic activity for hydrogen evolution of MFe_2O_4 (M = Cu, Ni) prepared by three different methods, *Journal of Photochemistry and Photobiology A: Chemistry*, 2018, **357**, 20–29.

4 M. B. Tahir, Microbial photoelectrochemical cell for improved hydrogen evolution using nickel ferrite incorporated WO_3 under visible light irradiation, *International Journal of Hydrogen Energy*, 2019, **44**, 17316–17322.

5 L. Li, J. Xu, S. Zhao, M. Mao and X. Li, Construction of p-n type heterojunction for effective photo-generated electron separation and visible light hydrogen evolution, *International Journal of Hydrogen Energy*, 2021, **46**, 1934–1944.

6 B. Xia, B. He, J. Zhang, L. Li, Y. Zhang, J. Yu, J. Ran and S.-Z. Qiao, TiO_2/$FePS_3$ S-Scheme Heterojunction for Greatly Raised Photocatalytic Hydrogen Evolution, *Advanced Energy Materials*, 2022, **12**, 2201449.

7 D. Liu, Z. Yan, P. Zeng, H. Liu, T. Peng and R. Li, In situ grown TiN/N-TiO_2 composite for enhanced photocatalytic H_2 evolution activity, *Front. Energy*, 2021, **15**, 721–731.

8 F. Dai, M. Zhang, M. Mi, Z. Li, J. Xing and L. Wang, Pt-surface oxygen vacancies coupling accelerated photo-charge extraction and activated hydrogen evolution, *Nano Res.*, 2023, **16**, 4736–4741.

9 T. Li, L. Zhang, X. Li, X. Wang and Z. Jin, Design and synthesis of phosphating bimetallic CeCo-MOF for substantially improved photocatalytic hydrogen evolution, *J. Mater. Chem. C*, 2022, **10**, 8750–8761.

10 Q. Yang, T. Wang, Z. Zheng, B. Xing, C. Li and B. Li, Constructing interfacial active sites in Ru/g-C_3N_4−x photocatalyst for boosting H_2 evolution coupled with selective benzyl-alcohol oxidation, *Applied Catalysis B: Environmental*, 2022, **315**, 121575.

11 Q. Xi, F. Xie, J. Liu, X. Zhang, J. Wang, Y. Wang, Y. Wang, H. Li, Z. Yu, Z. Sun, X. Jian, X. Gao, J. Ren, C. Fan and R. Li, In Situ Formation $ZnIn_2S_4$/Mo_2TiC_2 Schottky Junction for Accelerating Photocatalytic Hydrogen Evolution Kinetics: Manipulation of Local

Coordination and Electronic Structure, *Small*, 2023, **19**, 2300717.

12 D. Zhang, M. Wang, G. Wei, R. Li, N. Wang, X. Yang, Z. Li, Y. Zhang and Y. Peng, High visible light responsive $ZnIn_2S_4/TiO_{2-x}$ induced by oxygen defects to boost photocatalytic hydrogen evolution, *Applied Surface Science*, 2023, **622**, 156839.

13 D. Peng, Y. Wang, H. Shi, W. Jiang, T. Jin, Z. Jin and Z. Chen, Fabrication of novel $Cu_2WS_4/NiTiO_3$ heterostructures for efficient visible-light photocatalytic hydrogen evolution and pollutant degradation, *Journal of Colloid and Interface Science*, 2022, **613**, 194–206.

14 C. Yuan, H. Lv, Y. Zhang, Q. Fei, D. Xiao, H. Yin, Z. Lu and Y. Zhang, Three-dimensional nanoporous heterojunction of CdS/np-rGO for highly efficient photocatalytic hydrogen evolution under visible light, *Carbon*, 2023, **206**, 237–245.

15 Y. Shen, D. Li, Y. Dang, J. Zhang,W. Wang and B.Ma,A Ternary Calabash Model Photocatalyst (Pd/MoP)/CdS for Enhancing H_2 Evolution under Visible Light Irradiation. Applied Surface Science 2021, **564**, 150432.

16 C. H. Hsu and F. Mansfeld, Technical Note: Concerning the Conversion of the Constant Phase Element Parameter Y0 into a Capacitance, *Corrosion*, 2001, **57**, 747–748.